CMS Physics Analysis Summary

Contact: cms-pag-conveners-higgs@cern.ch 2013/07/22

Search for a non-standard-model Higgs boson decaying to a pair of new light bosons in four-muon final states

The CMS Collaboration

Abstract

Results are reported from a search for non-standard-model Higgs boson decays to pairs of new light bosons, each of which decays into the $\mu^+\mu^-$ final state. The data set corresponds to an integrated luminosity of $20.65\,\text{fb}^{-1}$ of proton-proton collisions at $\sqrt{s} = 8$ TeV, recorded by the CMS experiment at the LHC in 2012. One event is observed after analysis selection requirements were applied. A model-independent upper limit on the product of the cross section times branching fraction times acceptance is derived. The results are applicable to a broad spectrum of new physics scenarios and are also compared with the predictions of two benchmark models, NMSSM and dark SUSY, as functions of a Higgs boson mass larger than $86\,\text{GeV}/c^2$ and of a new light boson mass within the range 0.25–$3.55\,\text{GeV}/c^2$.

1 Introduction

The observation of a Higgs-like boson [1, 2] with a mass near 125 GeV/c^2 in searches for the standard model (SM) Higgs boson [3–5] at the Large Hadron Collider (LHC) raises the critical question of whether the new particle is in fact the SM Higgs boson. The precision of the comparisons of the new particle's production and decay properties with the final states predicted by the SM will improve with additional data. However, distinguishing a true SM Higgs boson from a non-SM Higgs bosons with couplings moderately different from the SM values will remain a challenge. Searches for non-SM Higgs boson production and decay modes are therefore particularly timely as they provide a complementary path, which in many cases can allow a discovery or rule out broad ranges of new physics scenarios with existing data.

We present an analysis that explores one of the non-SM decay modes of Higgs boson (h), which includes production of two new light bosons (a), each of which subsequently decay to boosted pairs of oppositely charged muons isolated from the rest of the event activity:

$$h \to 2a + X \to 4\mu + X,$$

where X denotes possible additional particles from cascade decays of a Higgs boson.

The Higgs boson production cross section may or may not be enhanced compared to the SM, depending on the specific parameters of the model. The search described in this paper is designed to be independent of the details of specific models, and the results can be interpreted in the context of other models predicting the production of the same final states. We also study two specific scenarios: next-to-minimal supersymmetric standard model (NMSSM) and supersymmentric models with additional "hidden" or "dark" sectors (Dark SUSY).

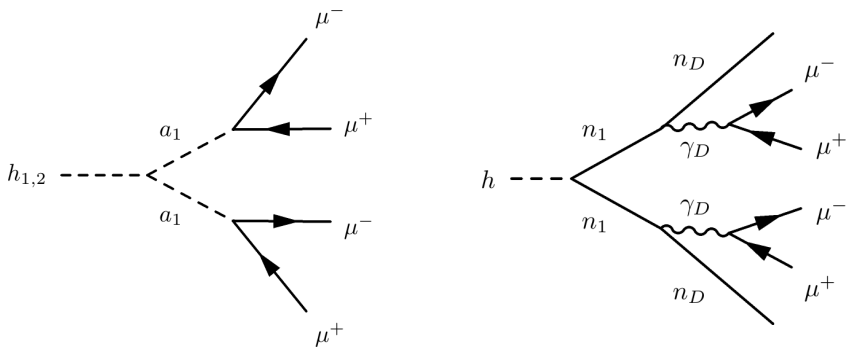

Figure 1: Left: Feynman diagram of the NMSSM benchmark process $h_{1,2} \to 2a_1 \to 4\mu$. Right: Feynman diagram of the dark-SUSY benchmark process $h \to 2n_1 \to 2n_D + 2\gamma_D \to 2n_D + 4\mu$.

The NMSSM [6–14] extends the minimal supersymmetric standard model (MSSM) [15–17] by an additional gauge singlet field under new $U(1)_{PQ}$ symmetry in the Higgs sector of the superpotential. Compared to the MSSM, the NMSSM naturally generates the mass parameter μ in the Higgs superpotential at the electroweak scale [18] and significantly reduces the amount of fine tuning required [19–21]. The Higgs sector of the NMSSM consists of 3 CP-even Higgs bosons $\mathrm{h}_{1,2,3}$ and 2 CP-odd Higgs bosons $\mathrm{a}_{1,2}$. In the NMSSM, the CP-even Higgs bosons h_1 and h_2 can decay via $\mathrm{h}_{1,2} \to 2\mathrm{a}_1$, where one of the h_1 or h_2 is a SM-like Higgs boson that could correspond to the newly observed state at the LHC with a mass near 125 GeV/c^2 [1, 2] and a_1 is a new CP-odd light Higgs boson [22–26]. The Higgs boson production cross section may differ substantially from that of the SM, depending on the parameters of a specific model. The new light boson a_1 couples weakly to SM particles, with the coupling to fermions proportional to the fermion mass, and can have a substantial branching fraction $\mathcal{B}(\mathrm{a}_1 \to \mu^+\mu^-)$ if its mass

is within the range $2m_\mu < m_{\mathrm{a}_1} < 2m_\tau$ [27, 28]. Feynman diagram of the NMSSM process $\mathrm{h}_{1,2} \to 2\mathrm{a}_1 \to 4\mu$ is shown in Fig. 1 (left).

The dark-SUSY models [29–31] are motivated by the excesses in positron spectra observed by satellite experiments [32, 33]. These models predict cold dark matter with a mass scale of $\sim 1\,\mathrm{TeV}/c^2$, which can provide the right amount of relic density due to the Sommerfeld enhancement in the annihilation cross section arising from a new $U(1)_D$ symmetry [34, 35]. In these models, $U(1)_D$ is broken, giving rise to light but massive dark photons γ_D that weakly couple to the SM particles via a small kinetic mixing [36–38] with photons. The lightest neutralino n_1 in the *visible* (as opposed to *hidden*) part of the SUSY spectrum is no longer stable and can decay via e.g. $\mathrm{n}_1 \to \mathrm{n}_D + \gamma_D$, where n_D is a light dark fermion (dark neutralino) that escapes detection. The SM-like Higgs boson can decay via $\mathrm{h} \to 2\mathrm{n}_1$, if $m_\mathrm{h} > 2m_{\mathrm{n}_1}$. The branching fraction $\mathcal{B}(\mathrm{h} \to 2\mathrm{n}_1)$ can vary from very small to large, bounded by the LHC measurements in the context of Higgs searches, since the bounds obtained at LEP can be circumvented [31]. The lack of an anti-proton excess in the measurements of the cosmic ray spectrum constrains the mass of γ_D to be $\leq \mathcal{O}(1)\,\mathrm{GeV}/c^2$ [39]. Assuming that γ_D can only decay to SM particles, the branching fraction $\mathcal{B}(\gamma_D \to \mu^+\mu^-)$ can be as large as 45%, depending on m_{γ_D} [31]. Feynman diagram of the dark-SUSY process $h \to 2n_1 \to 2n_D 2\gamma_D \to 2n_D 4\mu$ is shown in Fig. 1 (right).

Previous searches for the pair production of new light bosons decaying into dimuons were performed at the Tevatron with a $4.2\,\mathrm{fb}^{-1}$ data sample [40] and more recently at the LHC with a $35\,\mathrm{pb}^{-1}$ [41], a $1.9\,\mathrm{fb}^{-1}$ [42] and $5.3\,\mathrm{fb}^{-1}$ [43] data samples. Associated production of the light CP-odd scalar bosons has been searched for at $\mathrm{e}^+\mathrm{e}^-$ colliders [44, 45] and the Tevatron [46]. Direct production of the a_1 has been studied at the LHC [47], but in the framework of NMSSM the sensitivity of these searches is limited by the typically very weak coupling of the a_1 to SM particles. The most stringent limits on the Higgs sector of the NMSSM are provided by the WMAP data [48] and LEP searches [49–51] ($m_{\mathrm{h}_1} > 86\,\mathrm{GeV}/c^2$). In the framework of dark SUSY, experimental searches for γ_D have focused on the production of dark photons at the end of SUSY cascades at the Tevatron [52–54] and the LHC [41]. This analysis is based on a data sample corresponding to an integrated luminosity of $20.1\,\mathrm{fb}^{-1}$ of proton-proton collisions at $\sqrt{s} = 8$ TeV collected by CMS detector in 2012.

2 The CMS detector

The analysis presented in this Letter uses experimental data collected by the Compact Muon Solenoid (CMS) experiment at the LHC in 2012. The central feature of the CMS apparatus is a superconducting solenoid of 6 m internal diameter, providing a magnetic field of 3.8 T. Within the superconducting solenoid volume are a silicon pixel and strip tracker, a lead tungstate crystal electromagnetic calorimeter, and a brass/scintillator hadron calorimeter. The inner tracker measures charged particles within the pseudorapidity range $|\eta| < 2.5$, where $\eta = -\ln[\tan(\theta/2)]$ and θ is the polar angle with respect to the direction of the counterclockwise proton beam that is the z-axis of the CMS reference frame. The tracker provides an impact parameter resolution of $\sim$15 μm and a transverse momentum (p_T) resolution of about 1.5% for 100 GeV/c particles. Muons are measured in gas-ionization detectors embedded in the steel return yoke. The muon detectors are made using the following technologies: drift tubes ($|\eta| < 1.2$), cathode strip chambers ($0.9 < |\eta| < 2.4$), and resistive-plate chambers ($|\eta| < 1.6$). Matching the muons to the tracks measured in the silicon tracker results in a transverse momentum resolution between 1 and 5% for p_T values up to 1 TeV/c. A more detailed description can be found in Ref. [55].

3 Data selection

The analysis is based on a data sample corresponding to an integrated luminosity of 20.65 fb^{-1} of proton-proton collisions at $\sqrt{s} = 8\,\text{TeV}$, obtained in 2012. The data were collected with a trigger selecting events containing at least two muons, one with $p_\text{T} > 17\,\text{GeV}/c$ and one with $p_\text{T} > 8\,\text{GeV}/c$. In the offline analysis, events are selected by requiring at least one primary vertex reconstructed with at least four tracks and with its z coordinate within 24 cm of the nominal collision point. Offline muon candidates are built particle flow (PF) algorithm [56]. The data are further selected by requiring at least four offline muon candidates with $p_\text{T} > 8\,\text{GeV}/c$ and $|\eta| < 2.4$; at least one of the candidates must have $p_\text{T} > 17\,\text{GeV}/c$ and be reconstructed in the central region, $|\eta| < 0.9$. Application of the selection requirements described above yields 1,745 events in the data. The trigger efficiency for the selected events is high (96–97%) and is nearly independent of the p_T and η of any of the four muons. The $|\eta| < 0.9$ requirement is tighter than that imposed by the trigger, but eliminates significant model dependence attributable to the reduced trigger performance in the forward region in the presence of multiple spatially close muons. This η requirement causes an overall reduction in the analysis acceptance of about 20%, as obtained in a simulation study with one of the NMSSM benchmark samples used in the analysis.

Next, oppositely charged muons are grouped into dimuons (a muon may be shared between several dimuons) if their pairwise invariant mass satisfies $m_{\mu\mu} < 5\,\text{GeV}/c^2$ and if either the fit of the two muon tracks for a common vertex has a χ^2 fit probability greater than 1% or the two muon tracks satisfy the cone size requirement $\Delta R(\mu^+,\mu^-) = \sqrt{(\eta_{\mu^+} - \eta_{\mu^-})^2 + (\phi_{\mu^+} - \phi_{\mu^-})^2} < 0.01$, where ϕ is the azimuthal angle in radians. The ΔR requirement compensates for the reduced efficiency of the vertex probability requirement for dimuons with very low mass ($m_{\mu\mu} \gtrsim 2m_\mu$), in which the two muon tracks are nearly parallel to each other at the point of closest approach.

Once all dimuons are constructed, only events with exactly two dimuons not sharing common muons are selected for further analysis. There is no restriction on the number of ungrouped *(orphan)* muons. We reconstruct $z_{\mu\mu}$, the projected z coordinate of the dimuon system at the point of the closest approach to the beam line, using the dimuon momentum measured at the common vertex and the vertex position. We ensure that the two dimuons originate from the same pp interaction by requiring $|z_{\mu\mu_1} - z_{\mu\mu_2}| < 1\,\text{mm}$. This selection is fully efficient for signal events while reducing the probability of selecting rare events with dimuons from two separate primary interactions.

To suppress backgrounds with dimuons coming from jets, we require that the dimuons be isolated from other activity in the event, using the criterion $I_{\mu\mu} < 2\,\text{GeV}/c$, where the isolation parameter of the dimuon system $I_{\mu\mu}$ is defined as the scalar sum of the transverse momenta of all additional charged tracks with $p_\text{T} > 0.5\,\text{GeV}/c$ within a cone of size $\Delta R = 0.4$ centered on the momentum vector of the dimuon system. Tracks used in the calculation of $I_{\mu\mu}$ must also have a z coordinate at the point of the closest approach to the beam line that lies within 1 mm of the z coordinate of the dimuon system. The $I_{\mu\mu}$ selection yields nine events in data and it suppresses the contamination from $\text{b}\bar{\text{b}}$ production by about a factor of 50 (measured in data) while rejecting less than 20% of the signal events (obtained from the simulation study).

Finally, we require that the invariant masses of the two reconstructed dimuons are compatible with each other within the detector resolution $|m_1 - m_2| < 0.13\,\text{GeV}/c^2 + 0.065 \times (m_1 + m_2)/2$, where $m_1 = m_{\mu\mu_1}$ and $m_2 = m_{\mu\mu_2}$. The numerical parameters in this last requirement correspond to at least five times the size of the core resolution in dimuon mass, including the differ-

ences in resolution in the central and forward regions. The signal inefficiency of this $m_1 \simeq m_2$ selection is less than 5% per event; it is due to QED final-state radiation and is unrelated to the detector resolution. No constraint is imposed on the four-muon invariant mass, in order to maintain the model independence of the analysis, in particular with respect to models resulting in cascade decays such as dark-SUSY, where an unknown fraction of the energy goes into the light dark fermions, which escape detection.

Table 1: Event selection efficiencies $\epsilon^{MC}_{\text{full}}(m_{\text{h}_1}, m_{\text{a}_1})$, as obtained from the full detector simulation, and the geometric and kinematic acceptances $\alpha_{\text{gen}}(m_{\text{h}_1}, m_{\text{a}_1})$ calculated using generator level information only, with statistical uncertainties for the NMSSM benchmark model. The experimental data-to-simulation scale factors are not applied.

m_{h_1} [GeV/c^2]	90	100	125	125	125	125	125	150
m_{a_1} [GeV/c^2]	2	2	0.25	0.5	1	2	3.55	2
$\epsilon^{MC}_{\text{full}}$ [%]	11.4 ± 0.1	13.8 ± 0.1	35.1 ± 0.2	22.6 ± 0.1	18.9 ± 0.1	18.2 ± 0.1	17.6 ± 0.1	21.5 ± 0.1
α_{gen} [%]	15.9 ± 0.1	19.3 ± 0.1	52.9 ± 0.2	32.0 ± 0.2	27.2 ± 0.2	26.3 ± 0.2	25.9 ± 0.2	32 ± 0.2
$\epsilon^{MC}_{\text{full}}/\alpha_{\text{gen}}$ [%]	71.7 ± 0.9	71.4 ± 0.8	66.4 ± 0.4	70.6 ± 0.6	69.6 ± 0.7	69.3 ± 0.7	68.2 ± 0.7	67.3 ± 0.6

Table 2: Event selection efficiencies $\epsilon^{MC}_{\text{full}}(m_{\text{h}}, m_{\gamma_D})$, as obtained from the full detector simulation, and the geometric and kinematic acceptances $\alpha_{\text{gen}}(m_{\text{h}}, m_{\gamma_D})$ calculated using generator level information only, with statistical uncertainties for a dark-SUSY benchmark model, as obtained from simulation. The experimental data-to-simulation scale factors are not applied.

m_{h} [GeV/c^2]	90	110	125	150
m_{γ_D} [GeV/c^2]		0.4		
ϵ_{full} [%]	2.4 ± 0.1	4.7 ± 0.1	6.8 ± 0.1	9.8 ± 0.1
α_{gen} [%]	3.5 ± 0.1	6.8 ± 0.1	9.9 ± 0.1	14.6 ± 0.1
$\epsilon_{\text{full}}/\alpha_{\text{gen}}$ [%]	68.9 ± 2.1	68.7 ± 1.5	68.1 ± 1.2	67.3 ± 0.9

To estimate the efficiency of the analysis to select a possible signal, we use the two benchmark models introduced earlier. The NMSSM samples are simulated with the PYTHIA 6.4.26 event generator [57] using MSSM Higgs boson production via gluon-gluon fusion $gg \to \text{H}^0_{\text{MSSM}}$, where the Higgs bosons are forced to decay via $\text{H}^0_{\text{MSSM}} \to 2\text{A}^0_{\text{MSSM}}$. The masses of H^0_{MSSM} and A^0_{MSSM} are set to the desired values for the h_1 mass and a_1 mass, respectively. Both A^0_{MSSM} bosons are forced to decay to a pair of muons. The dark-SUSY samples are simulated with the MADGRAPH 4.5.2 event generator [58] using SM Higgs boson production via gluon-gluon fusion $gg \to \text{h}_{\text{SM}}$, where the mass of h_{SM} is set to the desired value for the h mass. The BRIDGE software [59] was used to implement the new physics model that forces the Higgs bosons h_{SM} to undergo a non-SM decay to a pair of neutralinos n_1, each of which decays $\text{n}_1 \to \text{n}_D + \gamma_D$, where $m_{\text{n}_1} = 10\,\text{GeV}/c^2$, $m_{\text{n}_D} = 1\,\text{GeV}/c^2$ and $m_{\gamma_D} = 0.4\,\text{GeV}/c^2$. Both dark photons γ_D are forced to decay to two muons, while both dark neutralinos n_D escape detection. The narrow width approximation is imposed by setting the widths of the Higgs bosons and dark photons to a small value ($10^{-3}\,\text{GeV}/c^2$). All benchmark samples are generated using the leading-order CTEQ6L1 [60] set of parton distribution functions (PDF), and are interfaced with PYTHIA 6.4.26 using the Z2 tune [61] for "underlying event" (UE) activity at the LHC and to simulate jet fragmentation, when applicable.

All events in the benchmark signal samples are processed through a detailed simulation of the CMS detector based on GEANT4 [62] and are reconstructed with the same algorithms used for

data analysis. Tables 1 and 2 show the event selection efficiencies $\epsilon_{\text{full}}^{MC}$ obtained using the simulated signal events for these two benchmark models using representative choices for masses of h, a_1 or γ_D. To provide a simple recipe for future reinterpretations of the results in the context of other models, we separately determine α_{gen}, the geometric and kinematic acceptance of this analysis calculated using generator level information only. It is defined with the criteria that an event contains at least four muons with $p_{\text{T}} > 8\,\text{GeV}/c$ and $|\eta| < 2.4$, with at least one of these muons having $p_{\text{T}} > 17\,\text{GeV}/c$ and $|\eta| < 0.9$. Tables 1 and 2 also show α_{gen} along with the ratio $\epsilon_{\text{full}}^{MC}/\alpha_{\text{gen}}$.

The model independence of the ratio $\epsilon_{\text{full}}^{MC}/\alpha_{\text{gen}}$ permits an estimate of the full event selection efficiency of this analysis for an arbitrary new physics model predicting the signature with a pair of new light bosons. The analysis makes some assumptions on the nature and characteristics of the new light bosons, namely that they should be of the same type, have a mass in range $2m_\mu < m_{\text{a}} < 2m_\tau$, decay to the $\mu^+\mu^-$ final state and not have a significant lifetime ($c\tau \lesssim 4$ cm). In addition, the two bosons, should be isolated and sufficiently separated from each other to avoid being vetoed by the isolation requirement. The acceptance α_{gen} may be calculated using only the generator level selection requirements that have been defined above. The full efficiency ϵ_{full} could then be calculated by multiplying α_{gen} by the ratio $\epsilon_{\text{full}}/\alpha_{\text{gen}} = r \times \epsilon_{\text{full}}^{MC}/\alpha_{\text{gen}} = 0.63 \pm 0.05$, where $r = \epsilon_{\text{full}}/\epsilon_{\text{full}}^{MC} = 0.93 \pm 0.08$ is a scale factor defined in Sec. 5 that accounts for differences between data and simulation, and $\epsilon_{\text{full}}^{MC}/\alpha_{\text{gen}} = 0.69 \pm 0.02$ is an average ratio over all of the benchmark points used. The systematic uncertainty in the ratio $\epsilon_{\text{full}}/\alpha_{\text{gen}}$ is around 7.9%. For reference, the individual systematics uncertainties in α_{gen} and ϵ_{full} are 3.0% and 8.4%, respectively, as discussed in Sec. 5.

4 Background estimation

The background contributions after final selections are dominated by $\text{b}\bar{\text{b}}$ and direct J/ψ pair production events. The leading part of the $\text{b}\bar{\text{b}}$ contribution is due to b-quark decays to pairs of muons via double semileptonic decays or resonances, i.e. ω, ρ, ϕ, J/ψ. A smaller contribution comes from events with one real dimuon and a second dimuon with a muon from a semileptonic b-quark decay and a charged hadron misidentified as another muon. The misidentification typically occurs due to the incorrect association of the track of the charged hadron with the track segments from a real muon in the muon system. The contribution of other SM processes has been found to be negligible (less than 0.1 events combined), for example low mass Drell–Yan production is heavily suppressed by the requirement of additional muons, and $\text{pp} \to \text{Z}/\gamma^* \to 4\mu$ production is suppressed by the requirement of small and mutually consistent masses of the dimuons [27]. The analysis is not sensitive to SM process $\text{pp} \to \text{H} \to \text{ZZ} \to 4\mu$ because the invariant mass of the dimuons is substantially lower than the Z mass.

Using data control samples, the $\text{b}\bar{\text{b}}$ background is modeled as a two dimensional (2D) template $B_{\text{b}\bar{\text{b}}}(m_1, m_2)$ in the plane of the invariant masses of the two dimuons in the selected events, where m_1 always refers to the dimuon containing a muon with $p_{\text{T}} > 17\,\text{GeV}/c$ and $|\eta| < 0.9$. For events with both dimuons containing such a muon, the assignment of m_1 and m_2 is random. As each b quark fragments independently, we construct the template describing the 2D probability density function as a Cartesian product $B_{17+8}(m_1) \times B_{8+8}(m_2)$, where the B_{17+8} and B_{8+8} templates model the invariant-mass distributions for dimuons with or without the requirement that the dimuon contains at least one muon satisfying $p_{\text{T}} > 17\,\text{GeV}/c$ and $|\eta| < 0.9$. This distinction is necessary as the shape of the dimuon invariant mass distribution depends on the transverse momentum thresholds used to select muons and whether the muons are in

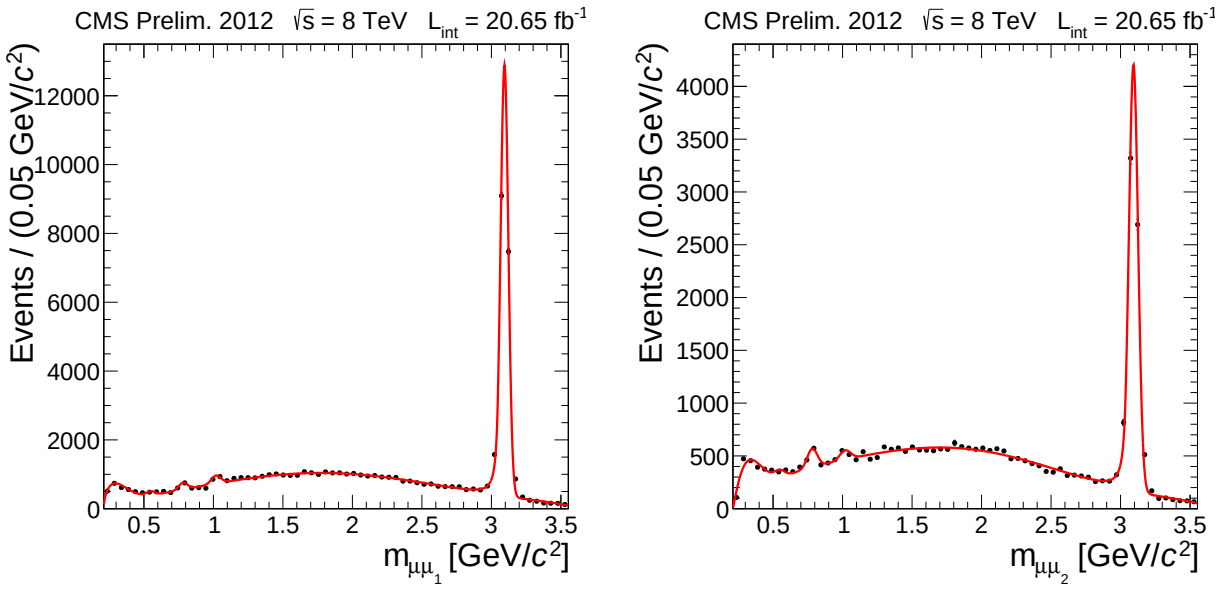

Figure 2: The B_{17+8} (left) and B_{8+8} (right) templates (solid lines) for dimuons obtained with background-enriched data (solid circles) samples.

the central ($|\eta| < 0.9$) or in the forward ($0.9 < |\eta| < 2.4$) regions, owing to the differences in momentum resolution of the barrel and endcap regions of the tracker. The B_{17+8} shape is measured using a data sample enriched in $\mathrm{b\bar{b}}$ events with exactly one dimuon and one orphan muon under the assumption that one of the b quarks decays to a dimuon containing at least one muon with $p_\mathrm{T} > 17\,\mathrm{GeV}/c$ and $|\eta| < 0.9$, while the other b quark decays semileptonically resulting in an orphan muon with $p_\mathrm{T} > 8\,\mathrm{GeV}/c$. For the B_{8+8} shape, we use a similar sample and procedure but only require the dimuon to have both muons with $p_\mathrm{T} > 8\,\mathrm{GeV}/c$, while the orphan muon has to have $p_\mathrm{T} > 17\,\mathrm{GeV}/c$ and $|\eta| < 0.9$. Both data samples used to measure background shapes are collected with the same trigger and with kinematic properties similar to those $\mathrm{b\bar{b}}$ events passing the selections of the main analysis. These event samples do not overlap the sample containing two dimuons that is used for the main analysis, and they have negligible contributions from non-$\mathrm{b\bar{b}}$ backgrounds. The B_{17+8} and B_{8+8} distributions, fitted with a parametric analytical function using a combination of Bernstein polynomials [63] and Crystal Ball functions [64] describing resonances, are shown as insets in Fig. 3 (left). Once the $B_{\mathrm{b\bar{b}}}(m_1, m_2)$ template is constructed, it is used to provide a description of the $\mathrm{b\bar{b}}$ background shape in the main analysis.

To validate the constructed $B_{\mathrm{b\bar{b}}}(m_1, m_2)$ template, we compare its shape with the distribution of the invariant masses m_1 vs. m_2 from events obtained with all standard selections except the requirement that each of the two reconstructed dimuons is isolated. Omitting the isolation requirement provides a high-statistics control sample of events with two dimuons highly enriched with $\mathrm{b\bar{b}}$ events. To avoid unblinding the search, the diagonal signal region is excluded in both the data and the template, i.e. the comparison has been limited to the data events that satisfy all analysis selections but fail the $m_1 \simeq m_2$ requirement. Distributions of m_1 and m_2 are consistent with the projections of the $B_{\mathrm{b\bar{b}}}(m_1, m_2)$ template on the respective axes normalized to the number of events in the data control sample. The sum of the m_1 and m_2 distributions agrees well with the sum of the template projections as shown in Fig. 3 (left).

To normalize the constructed $B_{\mathrm{b\bar{b}}}(m_1, m_2)$ template, we use the data events that satisfy all analysis selections, but fail the $m_1 \simeq m_2$ requirement. These selections yield eight events in the

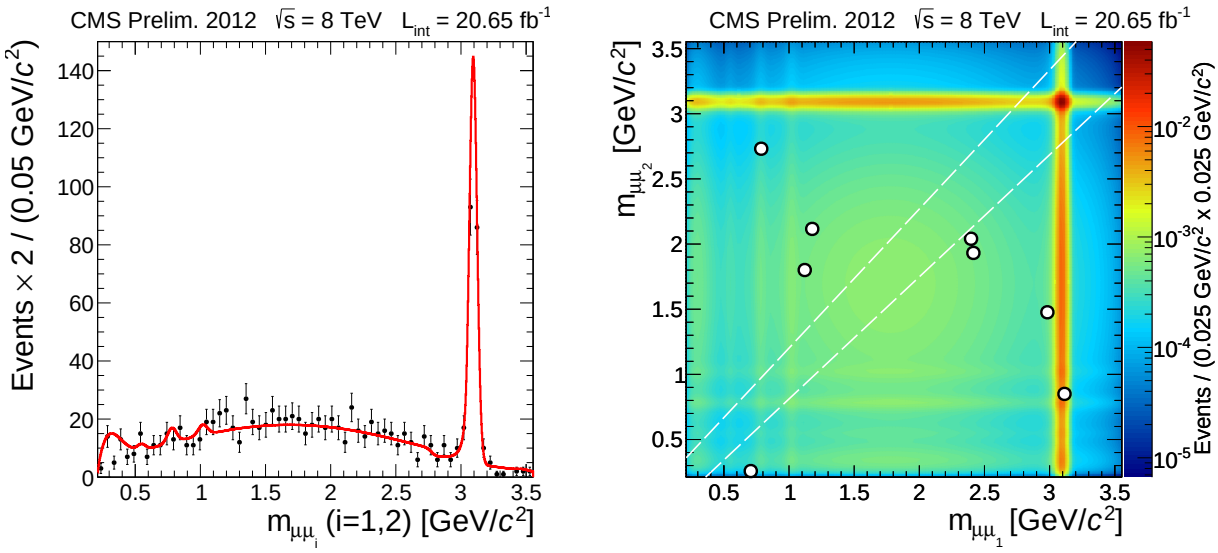

Figure 3: Left: Comparison of the data (solid circles) failing the $m_{\mu\mu_1} \simeq m_{\mu\mu_2}$ requirement in the control sample where no isolation requirement is applied to reconstructed dimuons with the prediction of the background shape model (solid line) scaled to the number of entries in the data. Right: Distribution of the invariant masses $m_{\mu\mu_1}$ vs. $m_{\mu\mu_2}$ for the isolated dimuon systems for the eight events in the data (shown as empty circles) surviving all selections except the requirement that these two masses fall into the diagonal signal region $m_{\mu\mu_1} \simeq m_{\mu\mu_2}$ (outlined with dashed lines). The intensity (color online) of the shading indicates the background expectation which is a sum of the $b\bar{b}$ and the direct J/ψ pair production contributions.

off-diagonal sideband region of (m_1, m_2) plane, leading, in the diagonal signal region, to an expected number of 1.8 ± 0.6 $b\bar{b}$ events, where the estimated uncertainty is dominated by the statistical uncertainty. These three events in the off-diagonal sidebands of the (m_1, m_2) plane are shown as empty circles in Fig. 3 (right).

The direct J/ψ pair production contribution is estimated using the simulation made with PYTHIA 8.108 event generator [65] and scaled to data (obtained in 2011 with 7 TeV) in a few regions of the invariant mass of the J/ψ pair. Then the estimate is rescaled using cross sections of double J/ψ process at 7 TeV and 8 TeV as reported by PYTHIA. This yields an estimate for the number of direct J/ψ pair produced events satisfying all analysis criteria of 2.0 ± 2.0 events.

The distribution of the total background expectation in the (m_1, m_2) plane is $B_{b\bar{b}}(m_1, m_2) + B_{2J/\psi}(m_1, m_2)$, i.e. a sum of the $b\bar{b}$ and the direct J/ψ pair production contributions. It is shown by the intensity of the shading in Fig. 3 (right). The background expectation in the diagonal signal region is 3.8 ± 2.1 events, where the uncertainty accounts for both statistical and systematic effects.

5 Systematic uncertainties

The selection efficiencies of offline muon reconstruction, trigger, and dimuon isolation criteria are obtained with simulation and have been corrected with scale factors derived from a comparison of data and simulation using $Z \to \mu\mu$ and J/$\psi \to \mu\mu$ samples. The scale factor per event is $r = 0.93 \pm 0.08$ (syst). It accounts for the differences in the efficiency of the trigger, the efficiency of the muon reconstruction and identification for each of the four muon candidates, and the combined efficiency of the isolation requirement for the two dimuon candidates. The

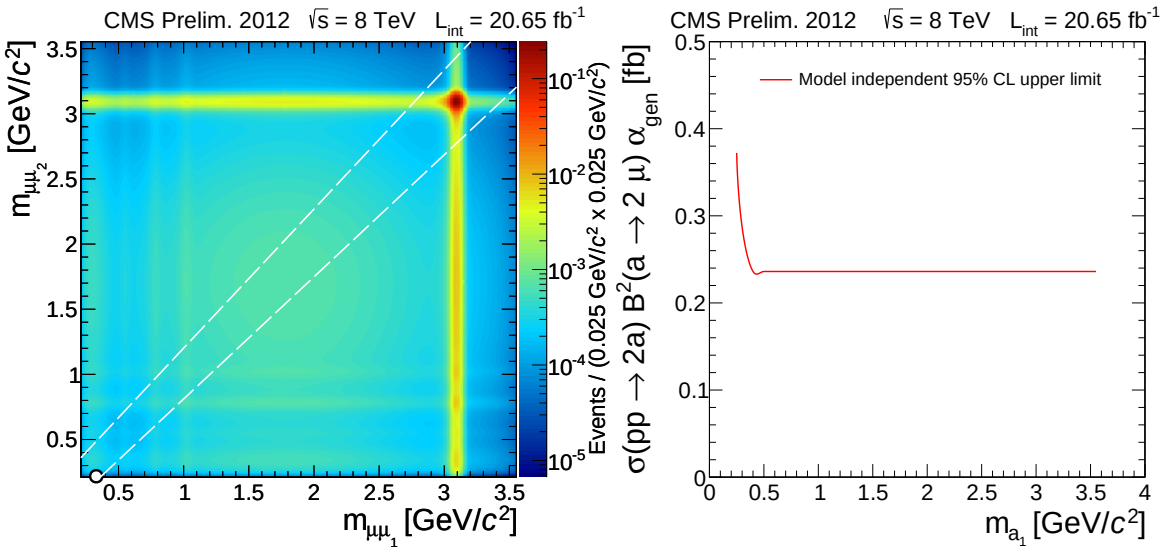

Figure 4: Left: Distribution of the invariant masses $m_{\mu\mu_1}$ vs. $m_{\mu\mu_2}$ for the isolated dimuon systems for the one event in the data (shown as empty circles) which survived all selection requirements. The intensity of the shading indicates the background expectation which is a sum of the $b\bar{b}$ and the direct J/ψ pair production contributions. Right: Model independent 95% CL upper limit on the product of the cross section times branching fraction times acceptance: $\sigma(pp \to 2a + X) \times \mathcal{B}^2(a \to 2\mu) \times \alpha_{gen}$.

correlations due to the presence of two close muons have been taken into account. The main systematic uncertainty is in the offline muon reconstruction (4%) which includes an uncertainty (1% per muon) to cover variations of the scale factor as a function of p_T and η of muons. Other systematic uncertainties include the uncertainty in the trigger (3.8%), dimuon isolation (negligible), dimuon reconstruction effects related to overlaps of muon trajectories in the tracker and in the muon system (3.5%), and dimuon mass shape, which affects the efficiency of the requirement that the two dimuon masses are compatible (1.5%). Also uncertainty in the LHC integrated luminosity of the data sample (4%) is included [66]. All the uncertainties quoted above, which relate to the final analysis selection efficiency for signal events, sum up to 7.9%. The uncertainties related to the parton distribution functions (PDFs) and the knowledge of the strong coupling constant α_s are estimated by comparing the PDFs in CTEQ6.6 [67] with those in NNPDF2.0 [68] and MSTW2008 [69] following the PDF4LHC recommendations [70]. Using the analysis benchmark samples, they are found to be 3% for the signal acceptance. Varying the QCD renormalization/factorization scales has a negligible effect. The total systematic uncertainty in the signal acceptance and selection efficiency is 8.4%.

6 Results

When the data satisfying all analysis selections were finally unblinded, one event was observed in the signal diagonal region. Masses of two dimuon systems in the selected event are shown in Fig. 4 (left) on $m_{\mu\mu_1}$ vs. $m_{\mu\mu_2}$ plane. The expected background in the diagonal signal region is 3.8 ± 2.1 events, where the uncertainty accounts for both statistical and systematic effects. This background includes contributions from $b\bar{b}$ production and direct J/ψ pair production.

For an arbitrary new physics model predicting the signature investigated in this analysis, the results can be presented as the 95% confidence level (CL) upper limit on $\sigma(pp \to 2a + X) \times$

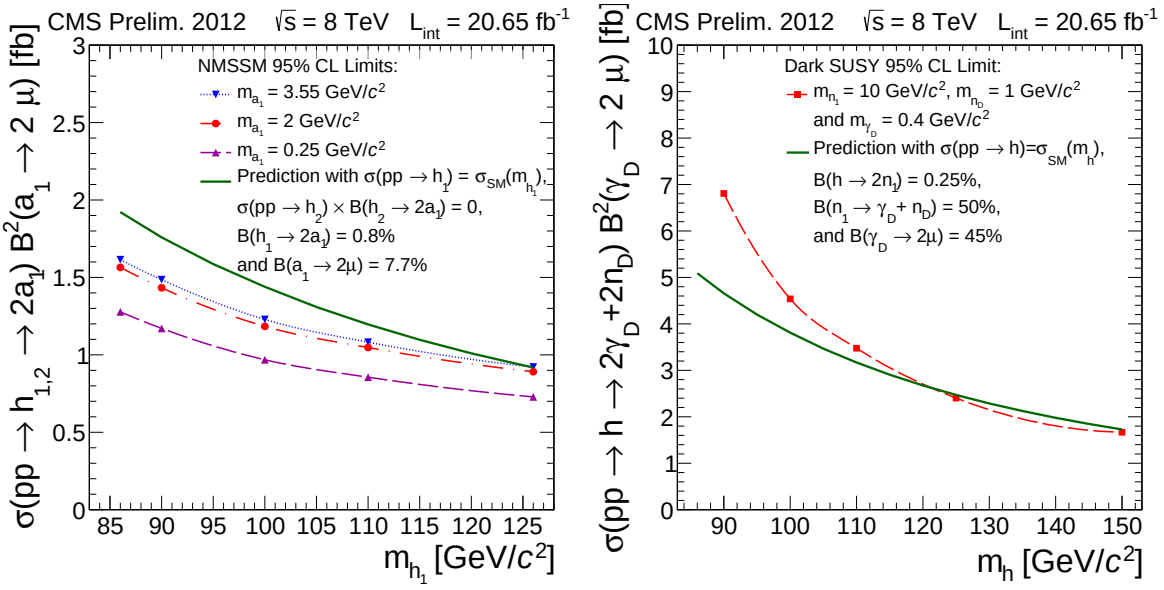

Figure 5: Left: The 95% CL upper limits as functions of m_{h_1}, for the NMSSM case, on $\sigma(\mathrm{pp} \to \mathrm{h}_{1,2} \to 2\mathrm{a}_1) \times \mathcal{B}^2(\mathrm{a}_1 \to 2\mu)$ with $m_{\mathrm{a}_1} = 0.25\,\mathrm{GeV}/c^2$ (dashed curve), $m_{\mathrm{a}_1} = 2\,\mathrm{GeV}/c^2$ (dash-dotted curve) and $m_{\mathrm{a}_1} = 3.55\,\mathrm{GeV}/c^2$ (dotted curve). As an illustration, the limits are compared to the predicted rate (solid curve) obtained using a simplified scenario with $\sigma(\mathrm{pp} \to \mathrm{h}_1) = \sigma_{\mathrm{SM}}(m_{\mathrm{h}_1})$ [71], $\sigma(\mathrm{pp} \to \mathrm{h}_2) \times \mathcal{B}(\mathrm{h}_2 \to 2\mathrm{a}_1) = 0$, $\mathcal{B}(\mathrm{h}_1 \to 2\mathrm{a}_1) = 0.8\%$, and $\mathcal{B}(\mathrm{a}_1 \to 2\mu) = 7.7\%$. The chosen $\mathcal{B}(\mathrm{a}_1 \to 2\mu)$ is taken from [28] for $m_{\mathrm{a}_1} = 2\,\mathrm{GeV}/c^2$ and NMSSM parameter $\tan\beta = 20$. Right: The 95% CL upper limit as a function of m_{h}, for the dark-SUSY case, on $\sigma(\mathrm{pp} \to \mathrm{h} \to 2\mathrm{n}_1 \to 2\mathrm{n}_D + 2\gamma_D) \times \mathcal{B}^2(\gamma_D \to 2\mu)$ with $m_{\mathrm{n}_1} = 10\,\mathrm{GeV}/c^2$, $m_{\mathrm{n}_D} = 1\,\mathrm{GeV}/c^2$ and $m_{\gamma_D} = 0.4\,\mathrm{GeV}/c^2$ (dashed curve). As an illustration, the limit is compared to the predicted rate (solid curve) obtained using a simplified scenario with SM Higgs boson production cross section $\sigma(\mathrm{pp} \to \mathrm{h}) = \sigma_{\mathrm{SM}}(m_{\mathrm{h}})$ [71], $\mathcal{B}(\mathrm{h} \to 2\mathrm{n}_1) = 0.25\%$, $\mathcal{B}(\mathrm{n}_1 \to \mathrm{n}_D + \gamma_D) = 50\%$, and $\mathcal{B}(\gamma_D \to 2\mu) = 45\%$. The chosen $\mathcal{B}(\gamma_D \to 2\mu)$ is taken from [31] for $m_{\gamma_D} = 0.4\,\mathrm{GeV}/c^2$.

$\mathcal{B}^2(\mathrm{a} \to 2\mu) \times \alpha_{\mathrm{gen}}$, where α_{gen} is the generator level kinematic and geometric acceptance defined in Sec. 3. The calculation uses the integrated luminosity $\mathcal{L} = 20.65\,\mathrm{fb}^{-1}$, as measured in data, and takes the ratio $\epsilon_{\mathrm{full}}/\alpha_{\mathrm{gen}} = 0.63 \pm 0.05$, derived in Sec. 3. The ratio includes the scale factor correcting for experimental effects not accounted for by the simulation, systematic uncertainties, and covers the variation in the ratio over all of the benchmark points used. The limit is shown in Fig. 4 (right). The limit is applicable to models with two pairs of muons coming from light bosons of the same type with a mass in range $0.25 < m_{\mathrm{a}} < 3.55\,\mathrm{GeV}/c^2$ where the new light bosons are typically isolated, spatially separated to not be vetoed by the isolation requirement and have no substantial lifetime. The efficiency of the selections in this analysis abruptly deteriorates if the light boson's decay vertex is more than ~ 4 cm from the beamline in the transverse plane.

We interpret these results in the context of the NMSSM and the dark-SUSY benchmark models, taking into account the dependence of the signal selection efficiencies on m_{h} and m_{a} (see Tab. 1 and Tab. 2), and derive 95% CL upper limits on the product of the cross section and branching fraction, using a Bayesian prescription. We also compare the derived experimental limits with a few simplified prediction scenarios. In the representative models, for any fixed combinations of m_{h} and m_{a} both the Higgs boson production cross section and the branching fractions can vary significantly, depending on the choice of parameters. In the absence of broadly accepted benchmark scenarios, we normalize the production cross sections in these examples to that of

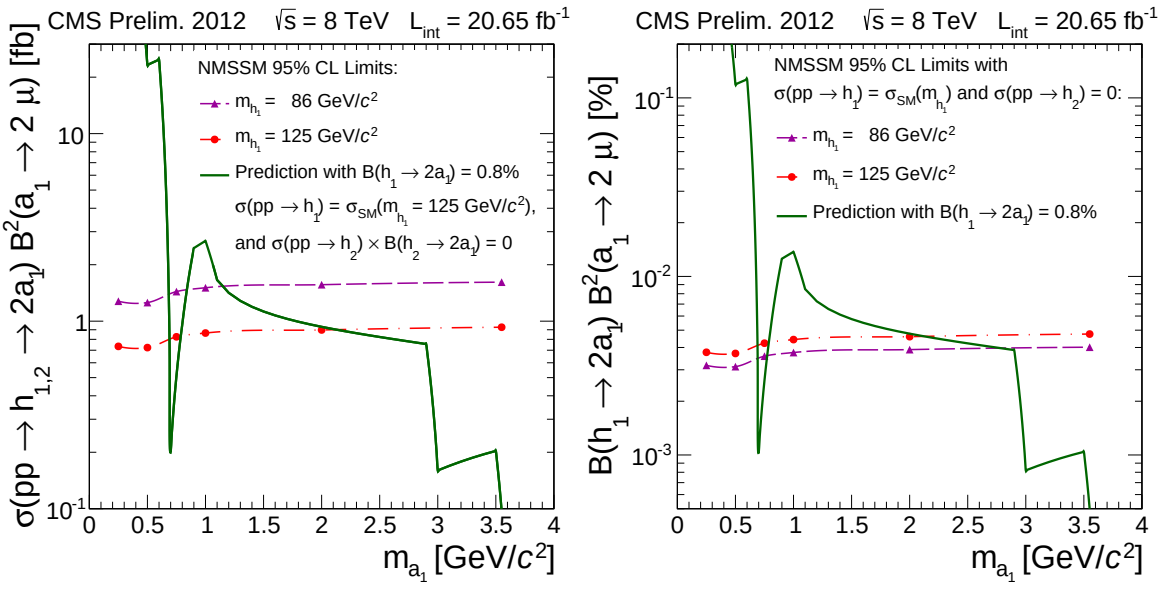

Figure 6: Left: The 95% CL upper limits as functions of m_{a_1}, for the NMSSM case, on $\sigma(\mathrm{pp} \to \mathrm{h}_{1,2} \to 2\mathrm{a}_1) \times \mathcal{B}^2(\mathrm{a}_1 \to 2\mu)$ with $m_{\mathrm{h}_1} = 86\,\mathrm{GeV}/c^2$ (dashed curve) and $m_{\mathrm{h}_1} = 125\,\mathrm{GeV}/c^2$ (dash-dotted curve). The limits are compared to the predicted rate (solid curve) obtained using a simplified scenario with $\mathcal{B}(\mathrm{h}_1 \to 2\mathrm{a}_1) = 0.8\%$, $\sigma(\mathrm{pp} \to \mathrm{h}_1) = \sigma_{\mathrm{SM}}(m_{\mathrm{h}_1} = 125\,\mathrm{GeV}/c^2)$ [71], $\sigma(\mathrm{pp} \to \mathrm{h}_2) \times \mathcal{B}(\mathrm{h}_2 \to 2\mathrm{a}_1) = 0$, and $\mathcal{B}(\mathrm{a}_1 \to 2\mu)$ as a function of m_{a_1} which is taken from [28] for NMSSM parameter $\tan\beta = 20$. Right: The 95% CL upper limits on $\mathcal{B}(\mathrm{h}_1 \to 2\mathrm{a}_1) \times \mathcal{B}^2(\mathrm{a}_1 \to 2\mu)$ with $m_{\mathrm{h}_1} = 90\,\mathrm{GeV}/c^2$ (dashed curve) and $m_{\mathrm{h}_1} = 125\,\mathrm{GeV}/c^2$ (dash-dotted curve) assuming $\sigma(\mathrm{pp} \to \mathrm{h}_1) = \sigma_{\mathrm{SM}}(m_{\mathrm{h}_1})$ [71] and $\sigma(\mathrm{pp} \to \mathrm{h}_2) \times \mathcal{B}(\mathrm{h}_2 \to 2\mathrm{a}_1) = 0$. The limits are compared to the predicted branching fraction (solid line) obtained using a simplified scenario with $\mathcal{B}(\mathrm{h}_1 \to 2\mathrm{a}_1) = 0.8\%$ and $\mathcal{B}(\mathrm{a}_1 \to 2\mu)$ as a function of m_{a_1} which is taken from [28] for NMSSM parameter $\tan\beta = 20$.

the SM Higgs boson [71].

For the NMSSM, the 95% CL upper limit is derived for $\sigma(\mathrm{pp} \to \mathrm{h}_{1,2} \to 2\mathrm{a}_1) \times \mathcal{B}^2(\mathrm{a}_1 \to 2\mu)$ as a function of m_{h_1} for three choices of m_{a_1} as shown in Fig. 5 (left) and as a function of m_{a_1} for three choices of m_{h_1} as shown in Fig. 6 (left). As m_{h_2} is unrestricted for any given m_{h_1}, we use $\epsilon_{\mathrm{full}}(m_{\mathrm{h}_2}) = \epsilon_{\mathrm{full}}(m_{\mathrm{h}_1})$ to simplify the interpretation. This is conservative since $\epsilon_{\mathrm{full}}(m_{\mathrm{h}_2}) > \epsilon_{\mathrm{full}}(m_{\mathrm{h}_1})$ if $m_{\mathrm{h}_2} > m_{\mathrm{h}_1}$, for any m_{a_1}. We also derive the 95% CL upper limit for $\mathcal{B}(\mathrm{h}_1 \to 2\mathrm{a}_1) \times \mathcal{B}^2(\mathrm{a}_1 \to 2\mu)$ as a function of m_{a_1} for three choices of m_{h_1} as shown in Fig. 6 (right) assuming that only h_1 gives a significant contribution to the final state considered in this analysis and has the production cross section of a SM Higgs boson, i.e. $\sigma(\mathrm{pp} \to \mathrm{h}_1) = \sigma_{\mathrm{SM}}(m_{\mathrm{h}_1})$ and $\sigma(\mathrm{pp} \to \mathrm{h}_2) \times \mathcal{B}(\mathrm{h}_2 \to 2\mathrm{a}_1) = 0$. For the NMSSM simplified prediction scenario we use $\mathcal{B}(\mathrm{a}_1 \to 2\mu)$ as a function of m_{a_1}, calculated in [28] for $\tan\beta = 20$ with no hadronization effects included in the $m_{\mathrm{a}_1} < 2m_\tau$ region. The branching fraction $\mathcal{B}(\mathrm{a}_1 \to 2\mu)$ is influenced by the $\mathrm{a}_1 \to s\bar{s}$ and $\mathrm{a}_1 \to gg$ channels. The significant structures in the predicted curves visible in Fig. 6 arise from the fact that $\mathcal{B}(\mathrm{a}_1 \to gg)$ varies rapidly in that region of m_{a_1}. The rapid variation in $\mathcal{B}(\mathrm{a}_1 \to gg)$ occurs when m_{a_1} crosses the internal quark loop thresholds. The representative value of $\mathcal{B}(\mathrm{a}_1 \to 2\mu)$ is equal to 7.7% for $m_{\mathrm{a}_1} \approx 2\,\mathrm{GeV}/c^2$. Finally, we choose $\mathcal{B}(\mathrm{h}_1 \to 2\mathrm{a}_1) = 0.8\%$, which yields predictions for the rates of dimuon pair events comparable to the obtained experimental limits.

In the case of the dark-SUSY model, the 95% CL upper limit is derived for $\sigma(\mathrm{pp} \to \mathrm{h} \to 2\mathrm{n}_1 \to 2\mathrm{n}_D + 2\gamma_D) \times \mathcal{B}^2(\gamma_D \to 2\mu)$ as a function of m_{h}. This limit is shown in Fig. 5 (right) for $m_{\mathrm{n}_1} =$

$10\,\text{GeV}/c^2$, $m_{\text{n}_D} = 1\,\text{GeV}/c^2$ and $m_{\gamma_D} = 0.4\,\text{GeV}/c^2$. For the dark-SUSY simplified prediction scenario we use the branching fraction $\mathcal{B}(\gamma_D \to 2\mu)$ close to its maximum at $m_{\gamma_D} = 0.4\,\text{GeV}/c^2$, of 45%, calculated in [31]. We also use $\mathcal{B}(\text{n}_1 \to \text{n}_D + \gamma_D) = 50\%$, allowing for other possible decays. Finally, we choose $\mathcal{B}(\text{h} \to 2\text{n}_1) = 0.25\%$, which yields predictions for the rates of dimuon pair events comparable to the obtained experimental limits.

7 Conclusions

A search for non-standard-model Higgs boson decays to pairs of new light bosons, which subsequently decay to pairs of oppositely charged muons ($\text{h} \to 2\text{a} + \text{X} \to 4\mu + \text{X}$) has been presented. The search is based on a data sample corresponding to an integrated luminosity of $20.65\,\text{fb}^{-1}$ collected by the CMS experiment in proton-proton collisions at $\sqrt{s} = 8\,\text{TeV}$ in 2012. One event with two dimuons of consistent single mass in the signal region was observed. An upper limit at 95% confidence level on the product of the cross section times branching fraction times acceptance is obtained. The limit is valid for new light-boson masses in the range $0.25 < m_{\text{a}} < 3.55\,\text{GeV}/c^2$ and for Higgs boson masses in the range $m_{\text{h}} > 86\,\text{GeV}/c^2$. Although results have been interpreted in the context of the NMSSM and the dark-SUSY benchmark models for $m_{\text{h}} < 150\,\text{GeV}/c^2$, it is possible to extend them by smoothly extrapolating the model-independent cross section limit to higher masses. The analysis has been designed as a quasi-model-independent search allowing interpretation of its results in the context of a broad range of new physics scenarios predicting the same type of signature. Presented results provide new best experimental limits for searches in this signature.

References

[1] ATLAS Collaboration, "Observation of a new particle in the search for the standard model Higgs boson with the ATLAS detector at the LHC", *Phys. Lett. B* **716** (2012) 1, doi:10.1016/j.physletb.2012.08.020, arXiv:1207.7214.

[2] CMS Collaboration, "Observation of a new boson at a mass of 125 GeV with the CMS experiment at the LHC", *Phys. Lett. B* **716** (2012) 30, doi:10.1016/j.physletb.2012.08.021, arXiv:1207.7235.

[3] F. Englert and R. Brout, "Broken symmetry and the mass of gauge vector mesons", *Phys. Rev. Lett.* **13** (1964) 321, doi:10.1103/PhysRevLett.13.321.

[4] P. W. Higgs, "Broken symmetries and the masses of gauge bosons", *Phys. Rev. Lett.* **13** (1964) 508, doi:10.1103/PhysRevLett.13.508.

[5] G. S. Guralnik, C. R. Hagen, and T. W. B. Kibble, "Global conservation laws and massless particles", *Phys. Rev. Lett.* **13** (1964) 585, doi:10.1103/PhysRevLett.13.585.

[6] P. Fayet, "Supergauge invariant extension of the Higgs mechanism and a model for the electron and its neutrino", *Nucl. Phys. B* **90** (1975) 104, doi:10.1016/0550-3213(75)90636-7.

[7] R. K. Kaul and P. Majumdar, "Cancellation of quadratically divergent mass corrections in globally supersymmetric spontaneously broken gauge theories", *Nucl. Phys. B* **199** (1982) 36, doi:10.1016/0550-3213(82)90565-X.

[8] R. Barbieri, S. Ferrara, and C. A. Savoy, "Gauge models with spontaneously broken local supersymmetry", *Phys. Lett. B* **119** (1982) 343, doi:10.1016/0370-2693(82)90685-2.

[9] H. P. Nilles, M. Srednicki, and D. Wyler, "Weak interaction breakdown induced by supergravity", *Phys. Lett.* **120** (1983) 346, doi:10.1016/0370-2693(83)90460-4.

[10] J.-M. Frere, D. R. T. Jones, and S. Raby, "Fermion masses and induction of the weak scale by supergravity", *Nucl. Phys. B* **222** (1983) 11, doi:10.1016/0550-3213(83)90606-5.

[11] J.-P. Derendinger and C. A. Savoy, "Quantum effects and SU(2)×U(1) breaking in supergravity gauge theories", *Nucl. Phys. B* **237** (1984) 307, doi:10.1016/0550-3213(84)90162-7.

[12] M. Drees, "Supersymmetric models with extended Higgs sector", *Int. J. Mod. Phys. A* **4** (1989) 3635, doi:10.1142/S0217751X89001448.

[13] M. Maniatis, "The next-to-minimal supersymmetric extension of the standard model reviewed", *Int. J. Mod. Phys. A* **25** (2010) 3505, doi:10.1142/S0217751X10049827, arXiv:0906.0777.

[14] U. Ellwanger, C. Hugonie, and A. M. Teixeira, "The next-to-minimal supersymmetric standard model", *Phys. Rept.* **496** (2010) 1, doi:10.1016/j.physrep.2010.07.001, arXiv:0910.1785.

[15] H. P. Nilles, "Supersymmetry, supergravity and particle physics", *Phys. Rept.* **110** (1984) 1, doi:10.1016/0370-1573(84)90008-5.

[16] S. P. Martin, "A supersymmetry primer", (1997). arXiv:hep-ph/9709356.

[17] D. J. H. Chung et al., "The soft supersymmetry breaking Lagrangian: theory and applications", *Phys. Rept.* **407** (2005) 1, doi:10.1016/j.physrep.2004.08.032, arXiv:hep-ph/0312378.

[18] J. E. Kim and H. P. Nilles, "The μ-problem and the strong CP-problem", *Phys. Lett. B* **138** (1984) 150, doi:10.1016/0370-2693(84)91890-2.

[19] J. A. Casas, J. R. Espinosa, and I. Hidalgo, "The MSSM fine tuning problem: a way out", *JHEP* **01** (2004) 008, doi:10.1088/1126-6708/2004/01/008, arXiv:hep-ph/0310137.

[20] R. Dermisek and J. F. Gunion, "Escaping the large fine tuning and little hierarchy problems in the next to minimal supersymmetric model and $h \to aa$ decays", *Phys. Rev. Lett.* **95** (2005) 041801, doi:10.1103/PhysRevLett.95.041801, arXiv:hep-ph/0502105.

[21] S. Chang, R. Dermisek, J. F. Gunion, and N. Weiner, "Nonstandard Higgs boson decays", *Ann. Rev. Nucl. Part. Sci.* **58** (2008) 75, doi:10.1146/annurev.nucl.58.110707.171200, arXiv:0801.4554.

[22] J. Ellis et al., "Higgs bosons in a nonminimal supersymmetric model", *Phys. Rev. D* **39** (1989) 844, doi:10.1103/PhysRevD.39.844.

[23] U. Ellwanger, M. Rausch de Traubenberg, and C. A. Savoy, "Particle spectrum in supersymmetric models with a gauge singlet", *Phys. Lett. B* **315** (1993) 331, doi:10.1016/0370-2693(93)91621-S, arXiv:hep-ph/9307322.

[24] U. Ellwanger, M. Rausch de Traubenberg, and C. A. Savoy, "Higgs phenomenology of the supersymmetric model with a gauge singlet", *Z. Phys. C* **67** (1995) 665, doi:10.1007/BF01553993, arXiv:hep-ph/9502206.

[25] B. A. Dobrescu, G. L. Landsberg, and K. T. Matchev, "Higgs boson decays to CP-odd scalars at the Tevatron and beyond", *Phys. Rev. D* **63** (2001) 075003, doi:10.1103/PhysRevD.63.075003, arXiv:hep-ph/0005308.

[26] D. J. Miller, R. Nevzorov, and P. M. Zerwas, "The Higgs sector of the next-to-minimal supersymmetric standard model", *Nucl. Phys. B* **681** (2004) 3, doi:10.1016/j.nuclphysb.2003.12.021, arXiv:hep-ph/0304049.

[27] A. Belyaev et al., "LHC discovery potential of the lightest NMSSM Higgs in the $h_1 \to a_1 a_1 \to 4\mu$ channel", *Phys. Rev. D* **81** (2010) 075021, doi:10.1103/PhysRevD.81.075021, arXiv:1002.1956.

[28] R. Dermisek and J. F. Gunion, "New constraints on a light CP-odd Higgs boson and related NMSSM ideal Higgs scenarios", *Phys. Rev. D* **81** (2010) 075003, doi:10.1103/PhysRevD.81.075003, arXiv:1002.1971.

[29] N. Arkani-Hamed, D. P. Finkbeiner, T. R. Slatyer, and N. Weiner, "A theory of dark matter", *Phys. Rev. D* **79** (2009) 015014, doi:10.1103/PhysRevD.79.015014, arXiv:0810.0713.

[30] M. Baumgart et al., "Non-Abelian dark sectors and their collider signatures", *JHEP* **04** (2009) 014, doi:10.1088/1126-6708/2009/04/014, arXiv:0901.0283.

[31] A. Falkowski, J. T. Ruderman, T. Volansky, and J. Zupan, "Hidden Higgs decaying to lepton jets", *JHEP* **05** (2010) 077, doi:10.1007/JHEP05(2010)077, arXiv:1002.2952.

[32] PAMELA Collaboration, "An anomalous positron abundance in cosmic rays with energies 1.5-100 GeV", *Nature* **458** (2009) 607, doi:10.1038/nature07942, arXiv:0810.4995.

[33] Fermi LAT Collaboration, "Measurement of separate cosmic-ray electron and positron spectra with the Fermi Large Area Telescope", *Phys. Rev. Lett.* **108** (2012) 011103, doi:10.1103/PhysRevLett.108.011103, arXiv:1109.0521.

[34] J. Hisano, S. Matsumoto, and M. M. Nojiri, "Explosive dark matter annihilation", *Phys. Rev. Lett.* **92** (2004) 031303, doi:10.1103/PhysRevLett.92.031303, arXiv:hep-ph/0307216.

[35] M. Cirelli, M. Kadastik, M. Raidal, and A. Strumia, "Model-independent implications of the $e^{\pm}$, $\bar{p}$ cosmic ray spectra on properties of dark matter", *Nucl. Phys. B* **813** (2009) 1, doi:10.1016/j.nuclphysb.2008.11.031, arXiv:0809.2409.

[36] B. Holdom, "Two U(1)'s and ϵ charge shifts", *Phys. Lett. B* **166** (1986) 196, doi:10.1016/0370-2693(86)91377-8.

[37] K. R. Dienes, C. F. Kolda, and J. March-Russell, "Kinetic mixing and the supersymmetric gauge hierarchy", *Nucl. Phys. B* **492** (1997) 104, doi:10.1016/S0550-3213(97)00173-9, arXiv:hep-ph/9610479.

[38] C. Cheung, J. T. Ruderman, L.-T. Wang, and I. Yavin, "Kinetic mixing as the origin of light dark scales", *Phys. Rev. D* **80** (2009) 035008, doi:10.1103/PhysRevD.80.035008, arXiv:0902.3246.

[39] PAMELA Collaboration, "PAMELA results on the cosmic-ray antiproton flux from 60 MeV to 180 GeV in kinetic energy", *Phys. Rev. Lett.* **105** (2010) 121101, doi:10.1103/PhysRevLett.105.121101, arXiv:1007.0821.

[40] D0 Collaboration, "Search for NMSSM Higgs bosons in the $h \to aa \to \mu\mu\mu\mu, \mu\mu\tau\tau$ channels using $p\bar{p}$ collisions at $\sqrt{s} = 1.96$ TeV", *Phys. Rev. Lett.* **103** (2009) 061801, doi:10.1103/PhysRevLett.103.061801, arXiv:0905.3381.

[41] CMS Collaboration, "Search for light resonances decaying into pairs of muons as a signal of new physics", *JHEP* **07** (2011) 098, doi:10.1007/JHEP07(2011)098, arXiv:1106.2375.

[42] ATLAS Collaboration, "Search for displaced muonic lepton jets from light Higgs boson decay in proton-proton collisions at $\sqrt{s} = 7$ TeV with the ATLAS detector", arXiv:1210.0435. , Submitted to Phys. Lett. B.

[43] CMS Collaboration, "Search for a non-standard-model Higgs boson decaying to a pair of new light bosons in four-muon final states", arXiv:1210.7619.

[44] CLEO Collaboration, "Search for very light CP-odd Higgs boson in radiative decays of $\Upsilon(1S)$", *Phys. Rev. Lett.* **101** (2008) 151802, doi:10.1103/PhysRevLett.101.151802, arXiv:0807.1427.

[45] BABAR Collaboration, "Search for dimuon decays of a light scalar boson in radiative transitions $\Upsilon \to \gamma A_0$", *Phys. Rev. Lett.* **103** (2009) 081803, doi:10.1103/PhysRevLett.103.081803, arXiv:0905.4539.

[46] CDF Collaboration, "Search for a very light CP-odd Higgs boson in top quark decays from $p\bar{p}$ Collisions at 1.96 TeV", *Phys. Rev. Lett.* **107** (2011) 031801, doi:10.1103/PhysRevLett.107.031801, arXiv:1104.5701.

[47] CMS Collaboration, "Search for a light pseudoscalar Higgs boson in the dimuon decay channel in pp collisions at $\sqrt{s} = 7$ TeV", *Phys. Rev. Lett.* **109** (2012) 121801, doi:10.1103/PhysRevLett.109.121801, arXiv:1206.6326.

[48] N. Jarosik et al., "Seven-year Wilkinson microwave anisotropy probe (WMAP) observations: sky maps,systematic errors, and basic results", *Astrophys. J. Suppl.* **192** (2011) 14, doi:10.1088/0067-0049/192/2/14, arXiv:1001.4744.

[49] OPAL Collaboration, "Decay mode independent searches for new scalar bosons with the OPAL detector at LEP", *Eur. Phys. J. C* **27** (2003) 311, doi:10.1140/epjc/s2002-01115-1, arXiv:hep-ex/0206022.

[50] OPAL Collaboration, "Search for a low mass CP-odd Higgs boson in e^+e^- collisions with the OPAL detector at LEP-2", *Eur. Phys. J. C* **27** (2003) 483, doi:10.1140/epjc/s2003-01139-y, arXiv:hep-ex/0209068.

[51] ALEPH, DELPHI, L3, OPAL, LEP Working Group for Higgs Boson Searches Collaboration, "Search for neutral MSSM Higgs bosons at LEP", *Eur. Phys. J. C* **47** (2006) 547, doi:10.1140/epjc/s2006-02569-7, arXiv:hep-ex/0602042.

[52] D0 Collaboration, "Search for dark photons from supersymmetric hidden valleys", *Phys. Rev. Lett.* **103** (2009) 081802, doi:10.1103/PhysRevLett.103.081802, arXiv:0905.1478.

[53] D0 Collaboration, "Search for events with leptonic jets and missing transverse energy in $p\bar{p}$ collisions at $\sqrt{s} = 1.96$ TeV", *Phys. Rev. Lett.* **105** (2010) 211802, doi:10.1103/PhysRevLett.105.211802, arXiv:1008.3356.

[54] CDF Collaboration, "Search for anomalous production of multiple leptons in association with W and Z bosons at CDF", *Phys. Rev. D* **85** (2012) 092001, doi:10.1103/PhysRevD.85.092001, arXiv:1202.1260.

[55] CMS Collaboration, "The CMS experiment at the CERN LHC", *JINST* **3** (2008) S08004, doi:10.1088/1748-0221/3/08/S08004.

[56] CMS Collaboration, "Performance of CMS muon reconstruction in pp collision events at $\sqrt{s} = 7$ TeV", *JINST* **7** (2012) P10002, doi:10.1088/1748-0221/7/10/P10002, arXiv:1206.4071.

[57] T. Sjöstrand, S. Mrenna, and P. Z. Skands, "PYTHIA 6.4 physics and manual", *JHEP* **05** (2006) 026, doi:10.1088/1126-6708/2006/05/026, arXiv:hep-ph/0603175.

[58] J. Alwall et al., "MadGraph/MadEvent v4: the new web generation", *JHEP* **09** (2007) 028, doi:10.1088/1126-6708/2007/09/028, arXiv:0706.2334.

[59] P. Meade and M. Reece, "BRIDGE: branching ratio inquiry / decay generated events", (2007). arXiv:hep-ph/0703031.

[60] J. Pumplin et al., "New generation of parton distributions with uncertainties from global QCD analysis", *JHEP* **0207** (2002) 012, arXiv:hep-ph/0201195.

[61] CMS Collaboration Collaboration, "Measurement of the Underlying Event Activity at the LHC with $\sqrt{s} = 7$ TeV and Comparison with $\sqrt{s} = 0.9$ TeV", *JHEP* **1109** (2011) 109, doi:10.1007/JHEP09(2011)109, arXiv:1107.0330.

[62] J. Allison et al., "Geant4 developments and applications", *IEEE Trans. Nucl. Sci.* **53** (2006) 270, doi:10.1109/TNS.2006.869826.

[63] S. Bernstein, "Demonstration du theoreme de Weierstrass fondee sur le calcul des probabilities", *Comm. Soc. Math. Kharkov* **13** (1912) 1.

[64] M. J. Oreglia, "A study of the reactions $\psi' \to \gamma\gamma\psi$". PhD thesis, Stanford University, 1980. SLAC Report SLAC-R-236, Appendix D.

[65] T. Sjöstrand, S. Mrenna, and P. Z. Skands, "A Brief Introduction to PYTHIA 8.1", *Comput. Phys. Commun.* **178** (2008) 852, doi:10.1016/j.cpc.2008.01.036, arXiv:0710.3820.

[66] CMS Collaboration, "Absolute Calibration of the Luminosity Measurement at CMS: Winter 2012 Update", CMS Physics Analysis Summary CMS-PAS-SMP-12-008, (2012).

[67] P. M. Nadolsky et al., "Implications of CTEQ global analysis for collider observables", *Phys. Rev. D* **78** (2008) 013004, doi:10.1103/PhysRevD.78.013004, arXiv:0802.0007.

[68] R. D. Ball et al., "A first unbiased global NLO determination of parton distributions and their uncertainties", *Nucl. Phys. B* **838** (2010) 136, doi:10.1016/j.nuclphysb.2010.05.008, arXiv:1002.4407.

[69] A. D. Martin, W. J. Stirling, R. S. Thorne, and G. Watt, "Parton distributions for the LHC", *Eur. Phys. J. C* **63** (2009) 189, doi:10.1140/epjc/s10052-009-1072-5, arXiv:0901.0002.

[70] M. Botje et al., "The PDF4LHC working group interim recommendations", (2011). arXiv:1101.0538.

[71] LHC Higgs Cross Section Working Group Collaboration, "Handbook of LHC Higgs cross sections: 1. Inclusive observables", (2011). arXiv:1101.0593.